Ground and satellite observations of substorm onset arcs

K. Shiokawa, K. Yago, K. Yumoto, K. Hayashi, D. G. Baishev, S. I. Solovyev, F. J. Rich, and S. B. Mende

Abstract: Auroral features and associated particles and fields are investigated for three auroral substorms (pseudo-breakups) observed at 19-20 MLT on December 30, 1994 and October 24 and 31, 2000. We identified the substorms using Pi 2 wave packets, positive/negative H variations at mid-/high-latitudes, and auroral brightenings in auroral images obtained by a ground all-sky camera and by the IMAGE FUV imager. The DMSP satellites crossed brightening arcs during the Pi 2 pulsations in the field-of-view of the ground camera at Fort Smith (67 MLAT), Canada, and Tixie (66 MLAT), Russia. The crossings were 1-2 hours duskside of the main onset local time. The brightening arcs were located at the equatorward boundary of the region 1 current and in the sunward convection region. The arcs corresponded to inverted-V accelerated electrons. From these observations, we suggest that the arc brightening occurs in the inner plasma sheet at the inner edge of the region 1 current source in the sunward convection region.

Key words: auroral initial brightening, precipitating particles, region 1 current, sunward convection.

1. Introduction

An auroral substorm is a manifestation of a magnetospheric substorm, which is a fundamental disturbance that releases the energy stored in the magnetosphere to the ionosphere. The onset mechanism of magnetospheric substorms is still controversial (see *Space Science Reviews, vol. 113, No. 1-2*, March 2004, for a review). Substorm onset is commonly described using the following two models.

The first is the near-Earth onset model, in which some instability in the nightside near-Earth plasma sheet inside 10 R_E causes a substorm (e.g., [17], [18], [12], and [5]). The fact that the auroral substorm starts from the most equatorward arc (e.g., [1] and [19]) supports this idea. [21] showed that the location of the auroral initial brightening was mapped inside 15 R_E in the magnetosphere. However, field-line mapping of the auroral brightening region to the magnetosphere is always ambiguous because of the tailward-stretched magnetic field configuration that is present during the substorm growth phase.

The other model of substorm onset is the near-Earth neutral line (NENL) model, in which the magnetic reconnection at 20-30 R_E in the tail causes the substorm (e.g., [14] and [3]). The NENL formation at radial distances of 20-30 R_E is supported by observations of the statistical flow-reversal location (e.g.,

[2], [23], and [20]) and of the detailed structure of the reconnection region (e.g., [24] and [27]). The mismatch between the auroral initial brightening (inside 10-15 R_E) and the reconnection region (20-30 R_E) may be explained by considering the braking of Earthward flow launched from the reconnection region as a generator of auroral brightening ([31]). [26] suggested that the two mechanisms (near-Earth instability and reconnection) may operate simultaneously in a coordinated way.

Particle and field signatures of the auroral initial brightening may be a key to identifying the source location of the brightening in the magnetosphere, and may help to verify the different models. For that purpose, several authors have compared auroral images and satellite particles and fields ([28]: meridian-scanning photometers and DMSP, [8]: ground auroral images and FAST, and [22]: satellite auroral images and FAST]. These studies indicate that the onset arc is located in the middle part or the equatorward edge of the electron precipitation region, and in the intense ion precipitation region, suggesting that the source is located in the inner part of the plasma sheet.

Despite these previous studies, simultaneous observation of auroral images and in situ plasma data at substorm onset is still very limited. In the ICS-8, we reported simultaneous measurements of substorm brightening arcs for three ground-satellite conjunction events, using auroral images and in situ particle, field-aligned current, and plasma convection data. Due to the limit of the total pages of this proceedings, we show only some parts of the measurements. The full descriptions of these three events were reported by [36], [34] and [37].

2. Observations

In this work, we use auroral images obtained by panchromatic all-sky TV cameras with image intensifier at Tixie (TIK, 71.6°N, 128.8°E, magnetic latitude (MLAT) = 66.0°) and at Fort Smith (FSM, 60.0°N, 248°E, 67.0°MLAT). The cameras take auroral images in visible wavelengths with a time resolution of 1-4 s. Details of the cameras are given by [29]. [35] and

[33] used the cameras for a detailed comparison of substorm arcs with Pi 2 pulsations.

Using auroral images over 4 years (1997-2000) at TIK and one month (December 1994 - January 1995) at FSM, we searched simultaneous observations of substorm-associated auroral arcs detected by the ground all-sky camera and auroral particle and field data obtained by the DMSP satellites in the field-of-view of the cameras. Only three events were available during which DMSP crossed the brightening arc within 10 min of the brightenings. This fact indicates the difficulty of obtaining simultaneous ground and satellite observations of substorm brightening arcs.
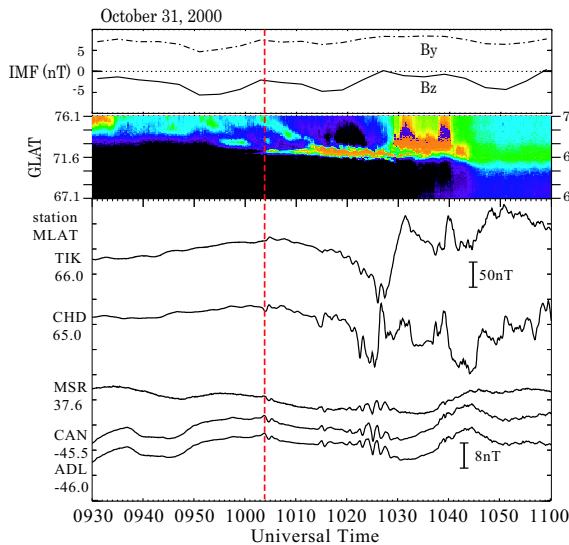

Fig. 1. Interplanetary magnetic field (IMF) variations obtained by the ACE spacecraft, time variations of auroral intensity in a north-south meridian obtained by the all-sky camera at Tixie (TIK), and H-component magnetic field variations at TIK, Chokurdakh (CHD), Moshiri (MSR), Canberra (CAN), and Adelaide (ADL) in the magnetic meridian of TIK, for the substorm brightening event of October 31, 2000. The magnetic field data are shown as 50 nT/division for TIK and CHD, and 8 nT/division for MSR, CAN, and ADL. The vertical red-dashed line indicates the time when the DMSP F12 satellite crossed the brightening arc, as shown in Figure 2.

Figure 1 is an example of IMF and ground auroral and magnetic field data during the ground-satellite conjunction event. It shows interplanetary magnetic field (IMF) variations obtained by the ACE spacecraft, auroral intensity variations in a north-south meridian (keogram) obtained by the all-sky camera at TIK, and H-component magnetic field variations at the CPMN stations at TIK, Chokurdakh (CHD), Moshiri (MSR), Canberra (CAN), and Adelaide (ADL) ([38]), for the substorm event on October 31, 2000, which was reported by [37]. IMF data is shifted 63 min by taking into account the travel time from the ACE spacecraft to the magnetopause. The all-sky images are converted to geographical coordinates, assuming an auroral altitude of 120 km. The keogram shows auroral intensity variations at a geographical longitude of TIK (128.8°E).

In Figure 1, IMF Bz measured by the ACE spacecraft at

$X = 219$ R_E was almost continuously southward (~ 0 to -5 nT), and By was duskward (> 5 nT) for 0930 – 1100 UT. In the keogram, the equatorward boundary of the auroral zone gradually shifts equatorward during the plotted interval. As indicated by the vertical dashed line, an auroral intensification took place at $\sim$1004 UT (18.5 MLT at TIK) at the equatorial boundary of the auroral zone at $\sim$66°MLAT ($\sim$72°GLAT). The DMSP F12 satellite crossed the arc at this time, as shown later. An equatorward-drifting aurora was observed simultaneously poleward of the brightening arc. However, auroral expansion was not observed in the keogram. Small magnetic field variations were seen in the high-latitude magnetograms at TIK and CHD at this time. Pi 2 pulsations with a coherent phase structure were identified in the midlatitude magnetic field data at MSR, CAN, and ADL. These features indicate that this auroral brightening is categorized as a pseudo-breakup. A major substorm took place at $\sim$1020–1040 UT, as characterized by an auroral expansion at TIK, high-latitude magnetic field variations and midlatitude Pi 2 pulsations.
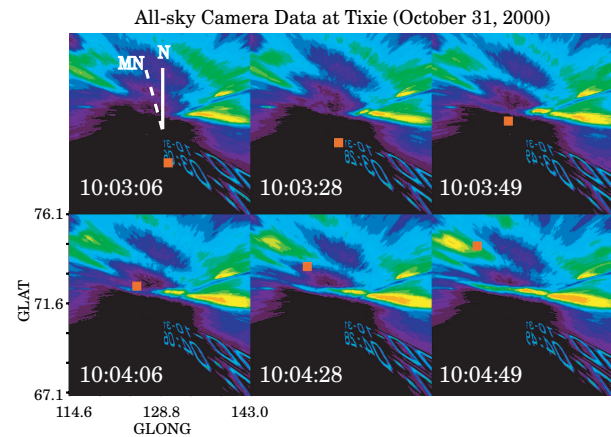

Fig. 2. Auroral images obtained at Tixie. Geographic north (N) and geomagnetic north (MN) are indicated in the 1003:06 UT image. Geographic latitude and longitude are indicated in the 1004:06 UT image. The orange squares indicate the footprint of the DMSP F12 spacecraft at an altitude of 120 km.

Figure 2 shows ground auroral images (1000 km $\times$ 1000 km) obtained at TIK from 1003:06 to 1004:49 UT. The images have been converted from the original all-sky coordinates to geographical coordinates by assuming an auroral altitude of 120 km. Geomagnetic north (MN) is 17° westward from geographic north (N). The image center is the zenith of TIK. The orange squares indicate the footprints of the DMSP F12 spacecraft at an altitude of 120 km.

In Figure 2, an auroral arc extends from east to west at 1003:49–1004:49 UT at a latitude of 72°N, which is the equatorward boundary of the auroral region. The arc completely expands to the west at 1004:49 UT. The arc width is less than 1 degree in latitude. The DMSP footprint crosses the western edge of the brightening arc from low to high latitudes at 1004:06 UT. Two auroral arcs in the NW-SE direction can be seen poleward of this brightening arc. They show continuous equatorward motion, as shown in Figure 1.
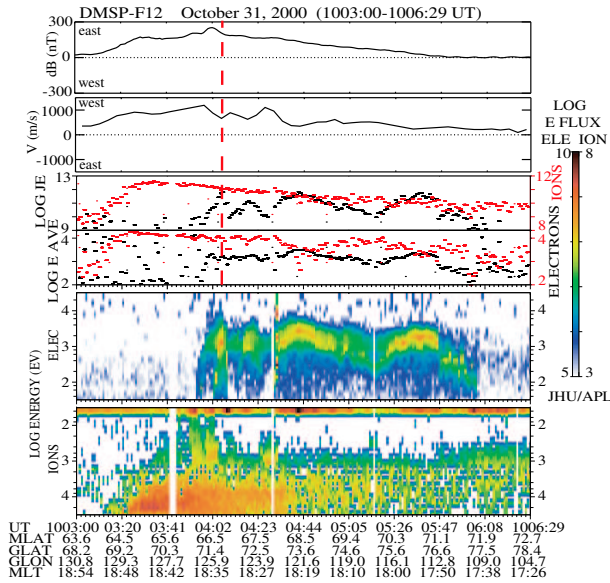
Fig. 3. Magnetic field, plasma speed, and precipitating particle data obtained by the DMSP F12 spacecraft at an altitude of 840 km at 1003:00–1006:29 UT on October 31, 2000. From top to bottom, magnetic field, plasma speed, electron (black) and ion (red) energy flux (eV/cm² s sr), average energy (eV), and electron and ion energy spectrograms. The dashed red line indicates the time (1004:06 UT) when the DMSP footprint crossed the brightening arc, as shown in Figure 2 (after [37]).
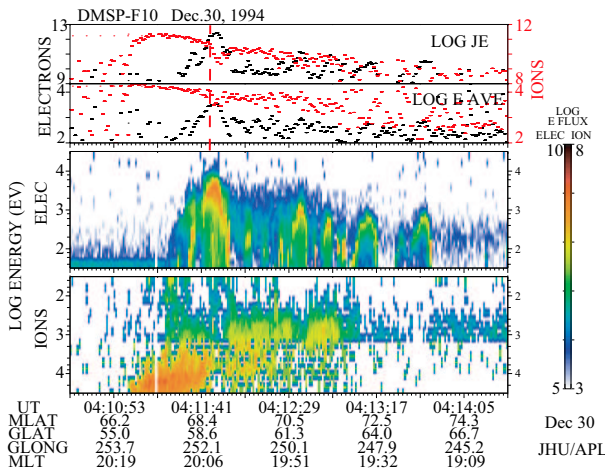

Fig. 4. Precipitating particle data obtained by the DMSP F10 spacecraft at an altitude of 840 km at 0410:30 UT – 0414:29 UT on December 30, 1994. From top to bottom, electron (black) and ion (red) energy flux (eV/cm² s sr), average energy (eV), and electron and ion energy spectrograms are shown. The vertical red-dashed line indicates the time (0411:48 UT) when the DMSP footprint crossed the brightening arc (after [36]).

The DMSP spacecraft is in circular polar orbit, and it observes precipitating electrons and ions, ion drift velocities, and magnetic field variations at an altitude of 840 km. These data from 1003:00 to 1006:29 UT on October 31, 2000, are shown in Figure 3. As shown by the vertical dashed line, the bright-
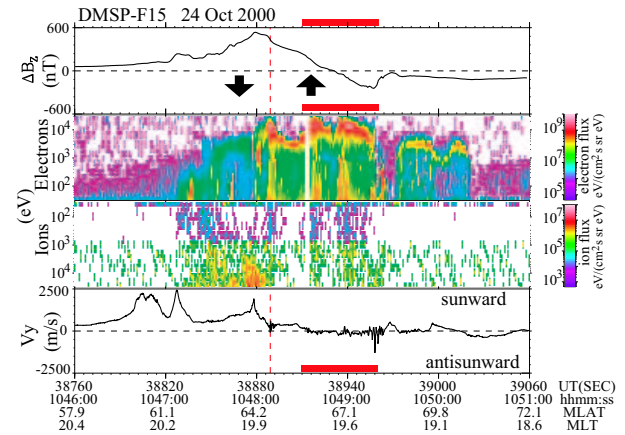

Fig. 5. Magnetic field, ion drift, and precipitating ion and electron data obtained by the DMSP F15 satellite at 1046:00–1051:00 UT on October 24, 2000. The vertical red-dashed line and horizontal red lines indicate satellite crossings of brightening arcs. The upward and downward arrows in the top panel indicate directions of the large-scale field-aligned currents inferred from the magnetic field data (after [34]).

ening arc corresponds to an electron inverted-V structure with a peak energy of ~1 keV at the equatorward edge of the electron precipitation region. The latitudinal width of the inverted-V structure is less than 1 degree, which is consistent with the observed arc width at Tixie. It is located ~3° (in latitude) poleward of the equatorward boundary of the ion precipitation region and ~6° equatorward of the poleward boundary of the electron precipitation region. The inverted-V structure is also located at the middle part of the energetic (> 1 keV) ion precipitation region.

In the top and second panels of Figure 3, we show magnetic field and ion drift velocities for the component perpendicular to the DMSP spacecraft's trajectory in the horizontal plane. The component can approximately be regarded as east-west component. For the magnetic field data, eastward magnetic field intensity increases (downward field-aligned current) from lower latitudes up to 66.5°MLAT, and then decreases (upward field-aligned current) to 72°MLAT. This feature is a typical pair of region 1 and 2 currents in the dusk sector ([15]). The auroral particles associated with the brightening arc (indicated by the vertical dashed line) are located at the equatorward edge of the upward region 1 field-aligned current, with a local enhancement of the current intensity.

The plasma velocity data obtained by the ion drift meter indicates that the whole region plotted in Figure 3 corresponds to the westward (sunward in this local time) convection region. The brightening arc at 66.6°MLAT is located in the middle of this sunward convection region. The arc corresponds to a local enhancement of velocity shear from west to east, which is a typical feature of auroral arcs (e.g., [4]).

Figure 4 shows the particle data for another ground-satellite conjunction event obtained by the DMSP F10 spacecraft from 0410:30 UT to 0414:29 UT on December 30, 1994. This event was reported in detail by [36] as the conjugate ground-satellite observation of a substorm brightening arc during a pseudo onset observed at FSM. As shown by the vertical red-dashed line,

the brightening arc corresponds to a clear electron inverted-V structure with a peak energy of ∼3 keV near the equatorward edge of the electron precipitation region. The inverted-V structure has a latitudinal width of ∼1 degree and is located about 2 degrees poleward of the equatorward boundary of the ion precipitation region and ∼5 degrees equatorward of the poleward boundary of the electron precipitation region. It is also located at the poleward boundary of the energetic (> 1 keV) ion precipitation region. The greatest ion energy flux region is located about 1 degree equatorward of the inverted-V structure. For this event, magnetic field and plasma drift data were not available.

Figure 5 shows the particle and field data for the third ground-satellite conjunction event obtained by the DMSP F15 spacecraft from 1046:00 UT to 1051:00 UT on October 24, 2000. This event was reported in detail by [34] as the conjugate ground-satellite observation of a sequence of substorm brightening arcs. During a 30-min interval at 1020-1050 UT, three Pi 2 wave packets and associated auroral brightenings are observed. The DMSP F15 satellite crossed the brightening arc just after the third brightening in the field of view of TIK. The DMSP F15 satellite crosses the most equatorward arc at ∼1048:15 UT, which brightened at the second Pi 2 onset. Intense accelerated electrons are observed around this time (1048:06–1048:12 UT), as indicated by the vertical dashed line. Then at ∼1048:40–1049:20 UT the satellite enters the region of westward-expanding auroras, which is brightened at the third Pi 2 onset. Two inverted-V type accelerated electrons are observed around this time (1048:30–1049:20 UT), as indicated by the horizontal red bars in Figure 5. The energy of these accelerated electrons reaches 10 keV. These accelerated electrons are located in the region of high-energy ion precipitation, which can be recognized at 61–68° MLAT (1047:00–1049:30 UT).

In the top panel of Figure 5, large-scale upward and downward field-aligned currents are observed, as shown by the black arrows. They are probably the region 1 (upward) and region 2 (downward) field-aligned currents in the evening sector ([15]). The brightening auroras indicated by the dashed line and horizontal bars are located in the region 1 upward field-aligned current. The ion drift data indicates that the plotted interval is mostly in the westward (sunward) convection region except for the latitudes higher than the electron precipitation region (>70 MLAT). The ion drift velocities in the onset arcs (indicated by the vertical red-dashed line and horizontal bars) show intense turbulences with peak-to-peak amplitudes up to ∼1000 m/s, while the background convection velocity is rather weak. It is noteworthy that the most equatorward arc (dashed line), which brightened after the second Pi 2 pulsation, is located at the equatorward edge of the region 1 current. This arc is located in the sunward convection region, where the convection velocity suddenly decreases from lower latitudes to higher latitudes. This decrease in convection velocity corresponds to converging poleward-directed Pedersen currents, which would give rise to the upward field-aligned currents of the arc. This decrease in convection velocity may also correspond to the duskward extension of the Harang discontinuity, though the velocity does not turn to negative. The intense westward drift at 59–62 MLAT (1046:30-1047:20 UT) is probably the Subauroral Ion Drift (SAID) associated with the high geomagnetic activity (e.g., [10] and [9]).

3. Summary and Discussion

We have shown particle and field features associated with auroral initial brightenings for three auroral substorms (pseudo-breakups) observed at 19-20 MLT on December 30, 1994 and October 24 and 31, 2000. The DMSP satellites crossed brightening arcs in the field-of-view of the ground all-sky cameras. All the crossings were 1-2 hours duskside of the main onset local time. The brightening arcs correspond to the inverted-V accelerated electrons at or near the equatorward edge of the electron precipitation region. They were located just poleward of the main ion precipitation region. They were located near the equatorward boundary of the region 1 current, in the sunward convection region, and in the localized turbulence region of ion drift velocity.
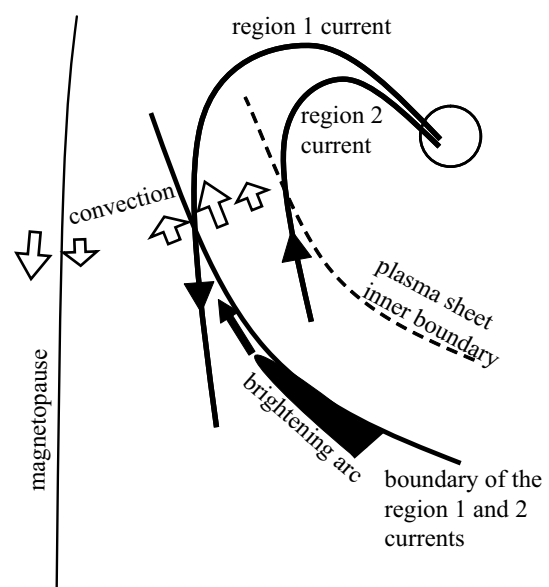

Fig. 6. Schematic picture of the observed features of the substorm brightening arc mapped to the equatorial plane of the magnetosphere. The observation was made at 1-2 hours duskside of the main onset local time. The brightening arc is located at the equatorward edge of the region 1 upward field-aligned current in the sunward convection region.

Figure 6 illustrates the observed features of the brightening arc mapped to the equatorial plane of the magnetosphere. For all the three events, the observations were made 1-2 hours duskside of the main onset local time. The brightening arc extended from the nightside just after the ground Pi 2 pulsation. The arc was located at the equatorward edge of the region 1 upward field-aligned current in the sunward convection region. This fact suggests that the onset occurs at the boundary of the region 1 and 2 current drivers in the magnetosphere.

According to MHD theory, the major field-aligned current drivers in the magnetosphere are particle inertia, pressure gradient, and temporal variation of flow shear (e.g., [13] and [11]). The pressure gradient force in the longitudinal direction from midnight to both evening and morning sectors possibly generates both the region 1 and 2 current systems ([32]), but mainly drives the region 2 current due to the inward gradient of the magnetic field. The partial ring current due to the gradient and

curvature of the magnetic field also drives the region 2 current system (e.g., [16] and [7]). These considerations suggest that the region 2 current drivers mainly act in the dipolar field region. The temporal development of the flow shear of the increase in westward flow with increasing latitude (inner part of the sunward convection belt) can also cause the region 2 downward current system in the evening sector. On the other hand, the temporal development of the flow shear of the decrease in westward flow with increasing latitude can drive the region 1 upward field-aligned current in the evening sector. This region 1 type flow shear is expected in the plasma sheet from the outer part of the sunward convection region to the antisunward convection region near the tail flank, as shown in Figure 6. The magnetospheric source of the most equatorward brightening arc is located at the boundary of these two current drivers.

[34] discussed the implication of the above observed facts in relation to the substorm models. The brightening arc is probably not connected directly to the lobe reconnection. However, these observations cannot differentiate between near-Earth onset models, i.e., flow braking ([30] and [31]), IMF northward turning and associated convection inhomogeneity ([18]), and near-Earth plasma sheet instability ([17], [6], and [25]). However, we would like to draw attention to the fact that the most equatorward arc that brightens at the substorm onset is not at the equatorward edge of the auroral oval and associated field-aligned current systems, but that the region 2 current system exists equatorward of the brightening arc.

It should be noted that our measurements were made 1–2 hours duskside of the main onset longitudes. For all the three events, the auroral arcs come from the east (nightside) in the field-of-view of the ground cameras. This motion is different from that in the onset region, where aurora simply brightens at the equatorward-most arc and expands poleward (e.g., [1] and [19]). [22] have shown, using the FAST particle data, that the auroral brightening at the onset longitude is caused by suprathermal electron precipitation. This fact suggests that at the exact onset longitude the brightening arc may not be the inverted-V accelerated electrons.

References

1. Akasofu, S. I., The development of the auroral substorm, *Planet Space Sci., 12*, 273, 1964.

2. Angelopoulos, V., et al., Statistical characteristics of bursty bulk flow events, *J. Geophys. Res., 99*, 21257, 1994.

3. Baker, D., N., T. I. Pulkkinen, V. Angelopoulos, W. Baumjohann, and R. L. McPherron, Neutral line model of substorms: past results and present view, *J. Geophys. Res., 101,* 12,975–13,010, 1996.

4. Burke, W. J., M. S. Gussenhoven, M. C. Kelly, D. A. Hardy, and F. J. Rich, Electric and magnetic field characteristics of discrete arcs in the polar cap, *J. Geophys. Res., 87*, 2431, 1982.

5. Cheng, C. Z., and A. T. Y. Lui, Kinetic ballooning instability for substorm onset and current disruption observed by AMPTE/CCE, *Geophys. Res. Lett., 25*, 4091–4094, 1998.

6. Cheng, C. Z., and S. Zaharia, MHD ballooning instability in the plasma sheet, *Geophys. Res. Lett., 31*, L06809, doi:10.1029/2003GL018823, 2004.

7. Crooker, N. U., and R. L. McPherron, On the distinction between the auroral electrojet and partial ring current systems, *J. Geophys. Res., 77*, 6886–6889, 1972.

8. Dubyagin, S. V., V. A. Sergeev, C. W. Carlson, S. R. Marple, T. I. Pulkkinen, and A. G. Yahnin, Evidence of near-Earth breakup location, *Geophys. Res. Lett., 30*, 10.1029/2002GL016569, 2003.

9. Foster, J. C., and H. B. Vo, Average characteristics and activity dependence of the subauroral polarization stream, *J. Geophys. Res., 107(A12)*, 1475, doi:10.1029/2002JA009409, 2002.

10. Galperin, Y., V. N. Ponomarev, and A. G. Zosimova, Plasma convection in the polar ionosphere, *Ann. Geophys., 30*, 1, 1974.

11. Haerendel, G., Field-aligned currents in the Earth's magnetosphere, in *Physics of Magnetic Flux Ropes, Geophys. Monogr. Ser.,* vol. 58, edited by C. T. Russell, E. R. Priest, and L. C. Lee, pp. 539–553, AGU, Washington, D. C., 1990.

12. Haerendel, G., Disruption, Ballooning or auroral avalanche – on the cause of substorms, *Proc. of the First International Conference on Substorms (ICS-1),* Kiruna, Sweden, pp.417–420, ESA, 1992.

13. Hasegawa, A., Generation of field aligned current during substorm, in *Dynamics of the Magnetosphere*, edited by S.-I. Akasofu, 529, D. Reidel, Norwell, Mass., 1979.

14. Hones, E. W., D. N. Baker, S. J. Bame, W. C. Feldman, J. T. Gosling, D. J. McComas, R. D. Zwickl, J. A. Slavin, E. J. Smith, and B. T. Tsurutani, Structure of the magnetotail at 220 R_E and its response to geomagnetic activity, *Geophys. Res. Lett., 11*, 5–8, 1984.

15. Iijima, T., and T. A. Potemura, Large-scale characteristics of field-aligned currents associated with substorm, *J. Geophys. Res., 83*, 599, 1978.

16. Kamide, Y., and N. Fukushima, Positive geomagnetic bays in evening high-latitudes and their possible connection with partial ring current, *Rep. Ionosph. Space Res. Jpn., 26*, 79–101, 1972.

17. Lui, A. T. Y., R. E. Lopez, B. J. Anderson, K. Takahashi, L. J. Zanetti, R. W. McEntire, T. A. Potemra, D. M. Klumpar, E. M. Greene, and R. Strangeway, Current disruptions in the near-Earth neutral sheet region, *J. Geophys. Res., 97*, 1461–1480, 1992.

18. Lyons, L. R., A new theory for magnetospheric substorms, *J. Geophys. Res., 100*, 19,069–19,081, 1995.

19. Lyons, L. R., I. O. Voronkov, E. F. Donovan, and E. Zesta, Relation of substorm breakup arc to other growth-phase auroral arcs, *J. Geophys. Res., 107*, 10.1029/2002JA009317, 2002.

20. Machida, S., Y. Miyashita, A. Ieda, A. Nishida, T. Mukai, Y. Saito, and S. Kokubun, GEOTAIL observations of flow velocity and north-south magnetic field variations in the near and mid-distant tail associated with substorm onsets, *Geophys. Res. Lett., 26(6)*, 635–638, 1999.

21. Murphree, J. S., R. D. Elphinstone, L. L. Cogger, and D. Hearn, Viking optical substorm signatures, in *Magnetospheric Substorms*, edited by J. R. Kan, T. A. Potemra, S. Kokubun, and T. Iijima, AGU Mono. 64, pp.241, 1991.

22. Mende, S. B., C. W. Carlson, H. U. Frey, L. M. Peticolas, and N. Østgaard, FAST and IMAGE-FUV observations of a substorm onset, *J. Geophys. Res., 108*, 10.1029/2002JA009787, 2003.

23. Nagai, T., M. Fujimoto, Y. Saito, S. Machida, T. Terasawa, R. Nakamura, T. Yamamoto, T. Mukai, A. Nishida, and S. Kokubun, Structure and dynamics of magnetic reconnection for substorm onsets with Geotail observations, *J. Geophys. Res., 103(A3)*, 4419–4440, 1998.

24. Nagai, T., I. Shinohara, M. Fujimoto, M. Hoshino, Y. Saito, S. Machida, and T. Mukai, Geotail observations of the Hall current system: Evidence of magnetic reconnection in the magnetotail, *J. Geophys. Res., 106(A11)*, 25,929–25,950, 2001.

25. Ohtani, S., A. T. Y. Lui, K. Takahashi, D. G. Mitchell, and T. Sarris, Ion dynamics and tail current intensification prior to dipolarization: The June 1, 1985, event, *J. Geophys. Res., 105(A11)*, 25,233–25,246, 2000.

26. Ohtani, S.-I., Substorm trigger processes in the magnetotail: Recent observations and outstanding issues, *Space Sci. Rev., 95*, 347, 2001.

27. Runov, A., et al., Current sheet structure near magnetic X-line observed by Cluster, *Geophys. Res. Lett., 30(11)*, 1579, doi:10.1029/2002GL016730, 2003.

28. Samson, J. C., L. R. Lyons, P. T. Newell, F. Creutzberg, and B. Xu, Proton aurora and substorm intensifications, *Geophys. Res. Lett., 19*, 2167, 1992.

29. Shiokawa, K., et al., Auroral observations using automatic instruments: Relations with multiple Pi 2 magnetic pulsations, *J. Geomag. Geoelectr., 48*, 1407, 1996.

30. Shiokawa, K., W. Baumjohann, and G. Haerendel, Braking of high-speed flows in the near-Earth tail, *Geophys. Res. Lett., 24*, 1179–1182, 1997.

31. Shiokawa, K., et al., High-speed ion flow, substorm current wedge, and multiple Pi 2 pulsations, *J. Geophys. Res., 103*, 4491–4508, 1998a.

32. Shiokawa, K., G. Haerendel, and W. Baumjohann, Azimuthal pressure gradient as driving force of substorm currents, *Geophys. Res. Lett., 25(7)*, 959–962, 1998b.

33. Shiokawa, K., K. Yumoto, and J. V. Olson, Multiple auroral brightenings and associated Pi 2 pulsations, *Geophys. Res. Lett., 29(11)*, 10.1029/2001GL014583, 2002.

34. Shiokawa, K., K. Yago, K. Yumoto, D. G. Baishev, S. I. Solovyev, F. J. Rich, and S. B. Mende, Ground and satellite observations of substorm onset arcs, *J. Geophys. Res., 110*, A12225, doi:10.1029/2005JA011281, 2005.

35. Solovyev, S. I., D. G. Baishev, E. S. Barkova, N. E. Molochushkin, and K. Yumoto, Pi2 magnetic pulsations as response on spatio-temporal oscillations of auroral arc current system, *Geophys. Res. Lett., 27(13)*, 1839–1842, 2000.

36. Yago, K., K. Shiokawa, K. Hayashi, and K. Yumoto, Auroral particles associated with a substorm brightening arc, *Geophys. Res. Lett., 32*, L06104, doi:10.1029/2004GL021894, 2005.

37. Yago, K., K. Shiokawa, K. Yumoto, D. G. Baishev, S. I. Solovyev, and F. J. Rich, Simultaneous DMSP, all-sky camera, and IMAGE FUV observations of a substorm onset arc, *submitted to Earth Planets Space*, 2006.

38. Yumoto, K., and the CPMN group, Characteristics of Pi 2 magnetic pulsations observed at the CPMN stations: A review of the STEP results, *Earth. Planets. Space., 53*, 981, 2001.